Eur. Phys. J. A **16**, 469–474 (2003)
DOI 10.1140/epja/i2002-10134-5

THE EUROPEAN PHYSICAL JOURNAL A

High-spin states in the ^{97}Tc nucleus

D. Bucurescu[1,a], A. Gadea[2], Ghe. Căta-Danil[1], I. Căta-Danil[1], M. Ivaşcu[1], N. Mărginean[1,b], C. Rusu[1,b], L. Stroe[1,b], and C.A. Ur[1,c]

[1] National Institute of Physics and Nuclear Engineering, P.O. Box MG-6, Bucharest 76900, Romania
[2] INFN, Laboratori Nazionali di Legnaro, Legnaro, Italy

Received: 22 November 2002 / Revised version: 20 December 2002 /
Published online: 18 March 2003 –
Communicated by C. Signorini

Abstract. High-spin states in the ^{97}Tc nucleus have been studied by in-beam γ-ray spectroscopy with the reaction ^{82}Se(^{19}F,4nγ) at 68 MeV incident energy. Excited states have been observed up to about 8 MeV excitation and spin $43/2\hbar$. The observed level scheme is compared with results of shell model calculations.

PACS. 21.10.Pc Single-particle levels and strength functions – 23.20.Lv Gamma transitions and level energies – 27.60.+j $90 \leq A \leq 149$

1 Introduction

The ^{97}Tc nucleus, with several protons between the semi-closed $Z = 40$ and the closed $Z = 50$ shells, and four neutrons above the $N = 50$ shell, may be considered as a typical "transitional" nucleus. It may develop some deformation, and therefore certain of its low-energy characteristics could be understood in terms of a rotational model. Alternatively, as is well known for such nuclei, a vibrational model can often describe the same features, especially if one looks mainly to states close to the yrast line. On the other hand, as this nucleus has not too many active particles (outside a closed shell "core"), realistic shell model calculations become feasible and should offer a reasonable understanding of all the observed features, giving in the same time a microscopic basis for the collective types of approach.

Low-spin states in ^{97}Tc have been previously observed at low excitation energies (below 1 MeV) by beta-decay [1], light-particle transfer reactions [2,3], and the (p,n) reaction [4,5]. Detailed data have been obtained up to about 2 MeV by a recent study with the (^{3}He,pnγ) reaction [6]. Higher-spin states have been observed in two studies with the (^{6}Li,3nγ) reaction [7,8], the highest spin observed in this way reaching $25/2\hbar$.

In the present work we extend the level scheme of ^{97}Tc up to an excitation energy of 8.3 MeV and spin $43/2\hbar$, by performing in-beam γ-ray spectroscopy via the heavy-ion fusion-evaporation reaction ^{82}Se(^{19}F,4nγ). After presenting the new results, the existing data on the structure of this nucleus are compared with shell model calculations.

2 Experimental techniques and results

High-spin states in ^{97}Tc were populated via the ^{82}Se(^{19}F,4nγ) reaction. A 68 MeV ^{19}F beam was delivered by the FN tandem Van de Graaff accelerator in Bucharest. The target was Se (94% enriched in ^{82}Se) with a thickness of 5 mg/cm^2 vacuum evaporated on a 2 mg/cm^2 Au foil. γ-γ and neutron-γ coincidences were measured with two intrinsic Ge detectors of 20% efficiency and a 1 litre NE213 scintillator detector, the later covering $\pm 28°$ in the forward direction. Gamma-ray angular distributions were measured both in the singles and neutron-coincident modes, by keeping one of the Ge detectors fixed at 145°, as a monitor, and moving the second one at six angles between 15° and 90°. The two sets of angular distributions have been compared in order to detect possible contaminants of the lines assigned to ^{97}Tc. A longer γ-γ coincidence run measured with the two detectors fixed at 90° and −45°, respectively, was used to deduce directional correlation from oriented states (DCO) ratios.

Gamma-ray transitions have been assigned to ^{97}Tc on the basis of their coincidence with previously known γ-rays [7,8]. For many of the new transitions we have also checked that the associated neutron multiplicity is 4; this was determined as the ratio between the intensity of the γ-ray in the spectrum in coincidence with neutrons and in the singles spectrum, respectively, after normalizing the values of this ratio to 4 for well-known γ-rays

[a] e-mail: bucurescu@tandem.nipne.ro
[b] *Present address:* INFN, Laboratori Nazionali di Legnaro, Legnaro, Italy.
[c] *Present address*: Università di Padova, Padova, Italy.

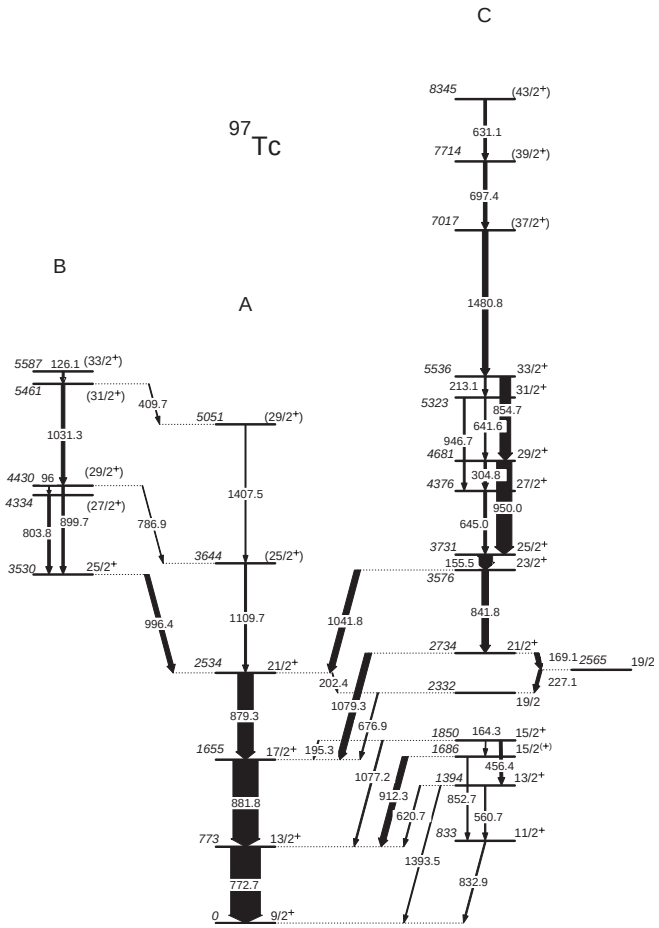

Fig. 1. Partial level scheme of ^{97}Tc, as resulted from the present experiment. The widths of the arrows are proportional to the γ-ray intensities (table 1). Spin and parity assignments are based on the properties of the transitions (table 1) and are also discussed in the text. Negative-parity levels established in ref. [8] up to a level $21/2^-$ at 3143 keV and also seen in this experiment are not shown in this figure.

of ^{97}Tc. Coincidence relationships have been studied on a symmetric matrix constructed from all γ-γ coincidence data. An asymmetric γ-γ coincidence matrix has been constructed from the data with the two detectors kept at fixed angles, and used to determine DCO ratios, defined as $R_{\rm DCO} = \frac{I_{\gamma_1}(\theta_1);\ \text{gated by}\ \gamma_2\ \text{at}\ \theta_2}{I_{\gamma_1}(\theta_2);\ \text{gated by}\ \gamma_2\ \text{at}\ \theta_1}$, with $\theta_1 = 45^\circ$ and $\theta_2 = 90^\circ$, respectively. In this geometry, if the gate is set on a pure quadrupole transition, then $R_{\rm DCO}$ should be 1.0 for a stretched quadrupole, and 0.5 for a stretched dipole, while if the gate is on a pure dipole transition, the values of $R_{\rm DCO}$ are 2.0 for a stretched quadrupole and 1.0 for a stretched dipole.

The level scheme determined in the present work on the basis of the γ-γ coincidences is shown in fig. 1. The placement of the transitions has been determined by their coincidence relationships, intensities and multipolarities (see table 1). In the lower part, the positive-parity yrast levels up to the $E_x = 3530$ keV, $25/2^+$ level, $E_x = 3644$ keV, $25/2^+$ level, and the levels shown in the right-hand side structure (labeled with C) up to the $E_x = 4681$ keV, $29/2^+$ level, coincide with levels determined in previous works [7,8]. The levels in structure A above 3644 keV, those in structure B above 3530 keV, and those from structure C above 4681 keV, are all found in this work.

Figure 2 shows selected gated spectra, which demonstrate the placement of the newly added transitions in the level scheme of fig. 1. Table 1 presents the characteristics of all the γ-ray transitions from this level scheme, such as relative intensities, angular-distribution Legendre polynomial coefficients and DCO ratios, as well as the assignment of each transition in the level scheme. There are a few transitions which almost coincide in energy with transitions from ^{95}Tc [9] or ^{96}Tc [10]; for these transitions the angular distributions could not be determined separately for each nucleus. On the other hand, in a couple of these cases one could determine the DCO ratio for the transition belonging to ^{97}Tc.

The transitions of 1109.7 and 1407.5 keV from the upper part of band A have a quadrupole multipolarity, therefore we have assumed that they are a continuation of the positive-parity $g_{9/2}$ weakly coupled band observed before in the (^{6}Li,3n) reaction [7,8]. Structure B is connected only to band A, therefore its parity has been tentatively assigned as positive. For the transitions added in structure C, we have also assumed positive parity due to the decay of this structure only to positive-parity states. For the lower states in this structure (below 5536 keV) J^π spin-parity values are proposed as based on indications from two decay branches, while for the upper states, for which only one decay γ-ray has been assigned, tentative values (J^π) are proposed.

The negative-parity band assigned in refs. [7,8] above the $1/2^-$ state at 96.5 keV (to be discussed below) has been observed with rather weak intensity and could not be continued at higher spins. This band has not been included in fig. 1.

3 Discussion and comparison with shell model calculations

3.1 General discussion

The lower part of the positive-parity level scheme, comprising both the levels shown in fig. 1 and other known low-spin states have already been discussed in various contexts. One had remarked, first of all, that the yrast cascade based on the $9/2^+$ ground state and some of the yrare states have strong similarities with the level scheme of ^{96}Mo, therefore they can be described by coupling of a $g_{9/2}$ proton to the collective states of the ^{96}Mo core [8]. Thus, for example, the two $25/2^+$ states known at the time (at 3530 and 3731 keV) were interpreted as a coupling of the $g_{9/2}$ quasiparticle to the 8_2^+ and 10_1^+ core states, respectively. In ref. [11], is discussed the evolution of this sequence (up to the spin 17/2) along the isotopic chain from ^{97}Tc to ^{105}Tc. In ^{97}Tc this band exhibits the features of

Table 1. Gamma-ray transitions in ^{97}Tc from the ^{82}Se(^{19}F,4nγ) reaction at 68 MeV. Unless specified, the DCO ratios are determined by gating on quadrupole transitions. Most of the γ-ray angular distributions have been obtained in coincidence with neutrons.

E_γ	I_γ	a_2/a_0	a_4/a_0	$R_{\rm DCO}$	Assignment		
(keV)	(rel. units)				E_i (keV)	E_f (keV)	$J_i^{\pi_i} \rightarrow J_f^{\pi_f}$
			Structure A				
772.7	100(1)	0.371(2)	−0.125(21)		772.7	0	$13/2^+ \rightarrow 9/2^+$
879.3	52.0(6)	0.318(25)	−0.117(31)	2.7(6)[c]	2533.9	1654.6	$21/2^+ \rightarrow 17/2^+$
881.8[b]	84.8(42)	0.308(17)	−0.116(22)	3.4(10)[c]	1654.6	772.8	$17/2+ \rightarrow 13/2^+$
1109.7	7.0(3)	0.290(26)	−0.146(30)	0.80(19)	3643.5	2533.9	$(25/2^+) \rightarrow 21/2^+$
1407.5	3.3(4)	0.33(11)	−0.31(14)		5051.3	3643.5	$(29/2^+) \rightarrow (25/2^+)$
			Structure B				
96.0	1.0(3)	0.02(48)	0.05(59)		4430.0	4334.1	$(29/2^+) \rightarrow (27/2^+)$
126.1	5.2(2)	−0.082(65)	−0.159(85)	0.34(7)	5587.4	5461.3	$(33/2^+) \rightarrow (31/2^+)$
803.8	8.7(12)	−0.075(88)	−0.038(115)	0.47(9)	4334.1	3530.3	$(27/2^+) \rightarrow 25/2^+$
899.7	8.1(15)	0.365(105)	−0.143(128)	2.8(6)[c]	4334.1	3530.3	$(29/2^+) \rightarrow 25/2^+$
1031.3[b]	12.0(10)	−0.207(32)	0.016(39)	0.58(8)	5461.3	4430.0	$(31/2^+) \rightarrow (29/2^+)$
			Transitions between structures A and B				
409.7	2.7(2)	−0.46(10)	0.11(14)	1.6(2)[c]	5461.3	5051.3	$(31/2^+) \rightarrow (29/2^+)$
786.9	2.3(4)	0.47(38)	0.34(47)		4430.0	3643.5	$(29/2^+) \rightarrow (25/2^+)$
996.4[a]	15.8(16)	0.345(17)	−0.082(22)		3530.3	2533.9	$25/2^+ \rightarrow 21/2^+$
			Structure C				
155.5	46.2(3)	−0.133(9)	−0.085(12)	0.45(5)	3731.2	3575.7	$25/2^+ \rightarrow 23/2^+$
164.3	–				1849.9	1685.6	$15/2^+ \rightarrow 15/2^{(+)}$
169.1[a]	14.6(5)	−0.175(72)	−0.062(80)		2733.9	2564.9	$21/2^+ \rightarrow 19/2$
213.1	5.9(3)	−0.237(18)	0.030(24)	0.48(8)	5535.9	5322.8	$33/2^+ \rightarrow 31/2^+$
227.1[a]	10.8(5)	0.096(51)	0.005(67)		2564.9	2331.5	$19/2 \rightarrow 19/2^+$
304.8	8.1(10)	−0.089(49)	0.038(67)	0.49(7)	4681.2	4376.2	$29/2^+ \rightarrow 27/2^+$
456.4[a]	9.6(7)	−0.370(65)	0.100(84)		1849.9	1393.5	$15/2^{(+)} \rightarrow 13/2^+$
560.7	4.4(6)	0.50(23)	0.43(28)		1393.5	832.9	$13/2^+ \rightarrow 11/2^+$
631.1	9.0(5)	0.337(21)	−0.104(29)	1.08(29)	8345.2	7714.1	$(43/2^+) \rightarrow (39/2^+)$
641.6	5.3(6)	−0.182(31)	0.019(42)	0.35(11)	5322.8	4681.2	$31/2^+ \rightarrow 29/2^+$
645.0	9.6(9)	−0.086(21)	−0.044(29)	0.43(9)	4376.2	3731.2	$27/2^+ \rightarrow 25/2^+$
697.4	12.0(6)	0.011(29)	0.106(38)	0.48(15)	7714.1	7016.4	$(39/2^+) \rightarrow (37/2^+)$
841.8	22.2(12)	−0.062(46)	0.016(63)	0.53(9)	3575.7	2733.9	$23/2^+ \rightarrow 21/2^+$
852.7	3.8(3)	–	–		1685.6	832.9	$15/2^{(+)} \rightarrow 11/2^+$
854.7	36.1(9)	0.279(34)	−0.058(46)	1.90(21)[c]	5535.9	4681.2	$33/2^+ \rightarrow 29/2^+$
946.7[a]	6.2(24)	−0.026(48)	−0.201(61)		5322.8	4376.2	$31/2^+ \rightarrow 27/2^+$
950.0	51.4(12)	0.295(22)	−0.073(29)	0.89(13)	4681.2	3731.2	$29/2^+ \rightarrow 25/2^+$
1480.8	18.8(7)	0.256(19)	−0.118(22)	1.55(20)[c]	7016.7	5535.9	$(37/2^+) \rightarrow (33/2^+)$
			Transitions between structures C and A				
195.3	3.7(3)	−0.035(60)	0.492(81)		1849.9	1654.6	$15/2^+ \rightarrow 17/2^+$
202.4	2.5(3)	0.062(95)	−0.021(127)		2533.9	2331.5	$21/2^+ \rightarrow 19/2$
620.7	4.0(3)	0.453(52)	−0.147(70)		1393.5	772.8	$13/2^+ \rightarrow 13/2^+$
676.9	4.2(4)	−0.344(40)	−0.026(50)		2331.5	1654.6	$19/2 \rightarrow 17/2^+$
832.9	4.8(3)	0.52(15)	0.09(19)		832.9	0	$11/2^+ \rightarrow 9/2^+$
912.3	20.0(11)	0.200(46)	−0.013(59)		1685.6	772.8	$15/2^{(+)} \rightarrow 13/2^+$
1041.8	20.2(10)	−0.250(51)	−0.034(27)	1.43(12)[c]	3575.7	2533.9	$23/2^+ \rightarrow 21/2^+$
1077.2	5.1(4)	−0.540(60)	−0.023(72)		1849.9	772.8	$15/2^+ \rightarrow 13/2^+$
1079.3	21.9(10)	0.302(17)	−0.078(23)	2.08(22)[c]	2733.9	1654.6	$21/2^+ \rightarrow 17/2^+$
1393.5	3.3(3)	0.355(37)	−0.216(90)		1393.5	0	$13/2^+ \rightarrow 9/2^+$

([a]) Only intensity (not the angular distribution coefficients) is corrected for the transition with the same energy in ^{96}Tc [10];
([b]) Only intensity (not the angular distribution coefficients) is corrected for the transition with the same energy in ^{95}Tc [9];
([c]) DCO ratio determined by gating on a dipole transition.

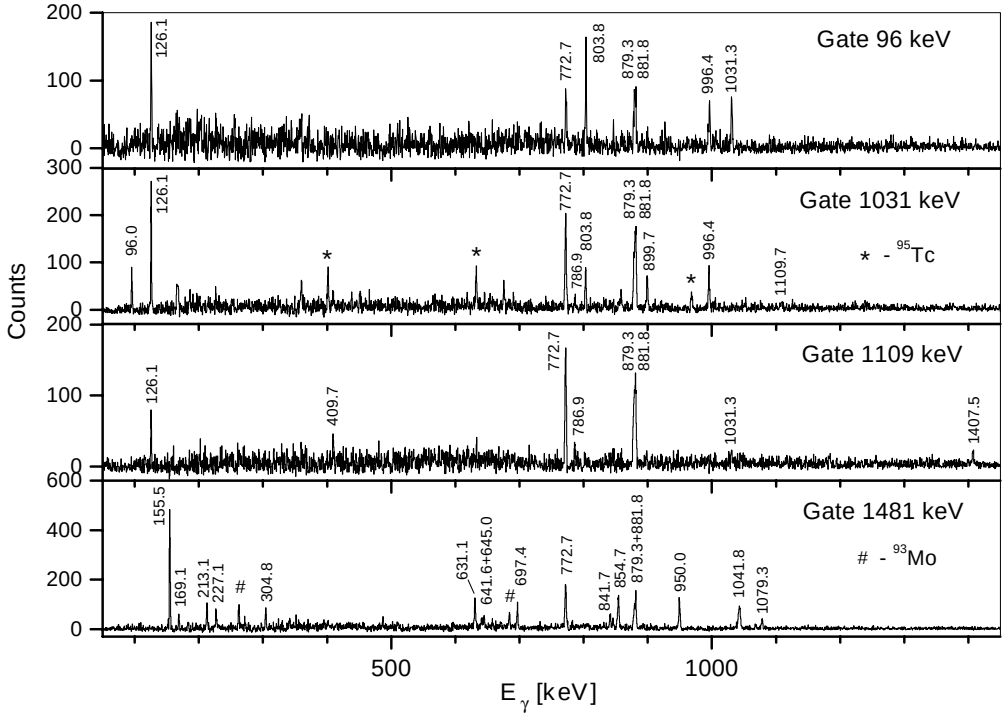

Fig. 2. Examples of gated γ-ray spectra which show the placement of the newly added transitions in the structures A, B and C from fig. 1.

a weak-coupling scheme, and evolves, with increasing N, towards a strong-coupling scheme.

For the lower-spin states, different interpretations were proposed on the basis of collective models. Thus, in ref. [8], the positive-parity states up to $21/2^+$ have been reasonably well described within the framework of the Interacting Boson-Fermion Model-1 (IBFM-1) [12], by coupling a $g_{9/2}$ proton to a ^{96}Mo core described by the Interacting Boson Model-1 [13]. We note that in this description the ^{96}Mo core has been assumed as having 3 bosons (^{90}Zr considered as inert core), therefore the maximum spin accounted for in ^{97}Tc is $21/2^+$. In a subsequent approach, a ^{96}Mo with 6 bosons has been chosen (valence nucleons counted relatively to a ^{100}Sn core) [14]. In both these approaches, only positions of yrast and near-yrast levels have been considered in the comparison between experiment and calculations.

In the recent study with the (^{3}He,pnγ) reaction, which provided a large number of low-spin states up to about 2 MeV excitation, an alternative approach has been used, based on the particle-rotor model [15]. Four Nilsson band structures of both parities have been identified up to about 2 MeV excitation, for calculations performed with a deformation $\delta = 0.24$, and thus the model accounted for a relatively large number of low-spin states and their electromagnetic de-excitation.

To understand the behaviour at higher spins, a possibility is to make a cranked-shell-model–type of analysis. This procedure assumes that the nucleus has some permanent deformation, which is justified by other model interpretations, as will be discussed below. Figure 3 displays

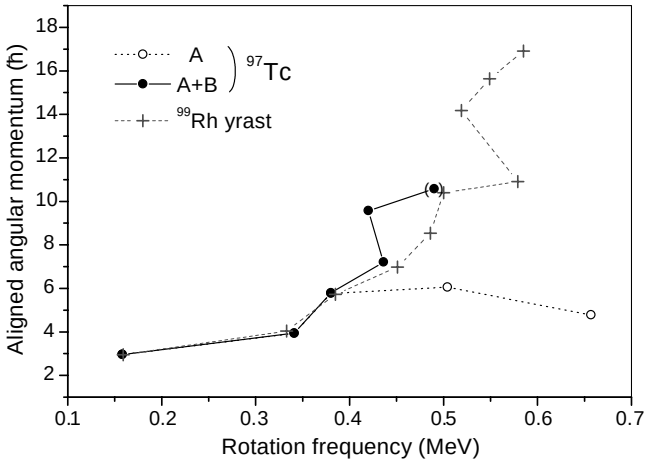

Fig. 3. Aligned angular momentum along the positive-parity structures A and B (fig. 1) of ^{97}Tc, and the positive-parity yrast structure in ^{99}Rh [17]. A Harris reference with $J_0 = 6.0\ \hbar^2\text{MeV}^{-1}$ and $J_1 = 15.7\ \hbar^4\text{MeV}^{-3}$ has been used. The plotted quantities have been calculated from the experimental data according to the formulas given in ref. [16]. The last point in the B sequence is shown only tentatively, since the $E2$ transition $33/2^+ \rightarrow 29/2^+$ has not been observed (fig. 1).

the aligned angular momentum along the two structures A and B from fig. 1, together with the same quantity for the positive-parity yrast structure of the isotonic nucleus ^{99}Rh [17]. The band A of fig. 1 has a gradual alignment process up to the $21/2^+$ state, then no gain in alignment is seen —this is the $g_{9/2}$ one-quasiparticle structure. After

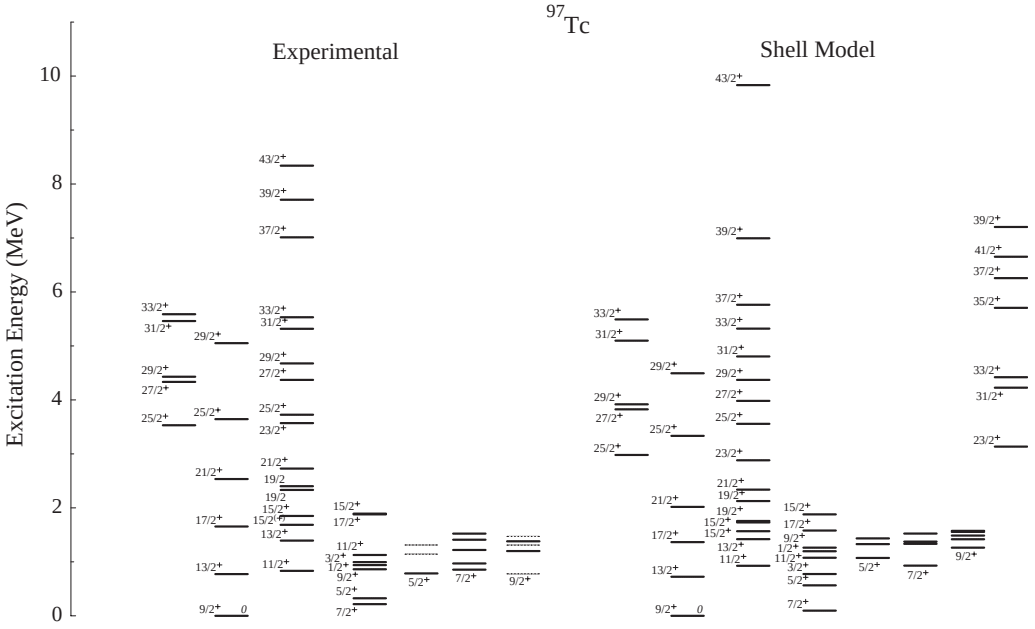

Fig. 4. Comparison of the positive-parity experimental levels of ^{97}Tc and the prediction of the shell model calculations described in the text. The experimental levels are from the works [6–8] and the present experiment.

the $21/2^+$ state, the yrast sequence continues with band B, which is seen to be similar to the yrast band of the isotone ^{99}Rh: in both nuclei there is an alignment gain of about $3.5\hbar$, around $\hbar\omega = 0.50$ MeV in ^{99}Rh, and 0.43 MeV in ^{97}Tc. Since the first proton crossing is blocked, this upbend is associated with the alignment of a $g_{7/2}$ neutron pair. Quasiparticle Routhians calculated for a deformation of $\beta_2 = 0.11$ and $\gamma = -15°$ as predicted for ^{99}Rh by total Routhian surface calculations, give a reasonable explanation of both this crossing and the higher one observed in ^{99}Rh at about 0.57 MeV and interpreted as due to the second proton crossing [17]. The lower frequency of the neutron crossing in ^{97}Tc may be due to a slightly smaller deformation. Note, however, that we did not observe the $E2$ transition $33/2^+ \rightarrow 29/2^+$ in the B structure, and this is why the last point in the backbending plot for structure B in fig. 3 is shown only tentatively. In this respect, ^{97}Tc appears different from ^{99}Rh, which shows an $E2$ band extending up to $49/2^+$.

Thus, different collective model approaches appear to account reasonably well for some of the characteristics determined until now at relatively low spins and excitation energies. None of them can account for all the observed levels. The present experiments provided many other levels in the higher-spin region as well. In order to understand this complicated structure we performed shell model calculations which are presented below.

3.2 Comparison with shell model calculations

The present shell model calculations have been performed with the code OXBASH [18]. The space has been chosen taking ^{88}Sr as inert core and the orbitals $[\pi(p_{1/2}, g_{9/2}); \nu(d_{5/2}, g_{7/2}, d_{3/2}, s_{1/2})]$ for the valence nucleons.

The single-particle energies (SPE) and two-body matrix elements (TBME), for this model space are from the interaction used by A. Brown and collaborators in the work of Mach *et al.* [19], optimized for $A = 95$–97 nuclei. The original space included the full fp-shell for protons but, due to the large dimension of the calculation for ^{97}Tc, we have used only the subset mentioned above. The interaction is based on the G-matrix potential of Hosaka, Kubo and Toki modified with the Gloeckner interaction to better describe nuclei in the $A = 96$ region [19–21]. The single-particle energies were deduced from the spectrum of $A = 95$–97 nuclei [19].

Figure 4 shows a comparison between the experimental levels of positive parity and the results of the shell model calculations. All experimentally known states with spin higher than $9/2^+$ have been shown, whereas the states of lower spin have been drawn only up to about 1.5 MeV (above this excitation energy there are little firm assignments [6]). One can see that the calculations account reasonably well for these levels both in number and general distribution in energy. The comparison in fig. 4 suggests that the calculated states $23/2_2^+$, $31/2_1^+$, $33/2_1^+$, $35/2_1^+$, $37/2_1^+$, $39/2_2^+$, $41/2_1^+$, have not been observed in the experiments. Above spin 33/2, the correspondence between the observed levels and the calculated ones becomes less reliable; also, the calculated state with spin 43/2 is rather high in energy. These discrepancies in the higher-spin region may reflect first of all the strong truncation of our space, namely, the exclusion of the neutron $h_{11/2}$ shell, and of the proton $f_{7/2}$, $f_{5/2}$, and $p_{3/2}$ shells. An additional reason may be also the need of breaking the $N = 50$ core at higher energies.

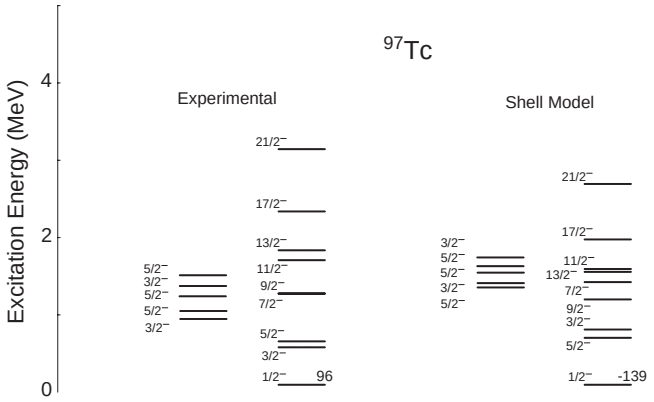

Fig. 5. Same as fig. 4, but for the negative-parity levels. The lowest calculated state, $1/2^-$, has been drawn at the experimental level position, but the calculated position with respect to the lowest $9/2^+$ level is indicated (see also the text). Some additional low-spin states shown on the left of the $1/2^-$ band correspond to the beginnings of rotational bands proposed in ref. [6]. Their possible calculated counterparts are also shown, but no one-to-one correspondence to the experimental levels has been made.

Figure 5 shows the comparison for the case of the negative-parity states. Again, the qualitative agreement is rather satisfactory, especially if one takes into account the fact that the $h_{11/2}$ neutron orbital has not been included in the calculations. One should remark, however, that the first negative-parity state, $1/2^-$, is predicted as ground state (139 keV below the $9/2^+$ state), whereas experimentally the situation is the reverse, with the $1/2^-$ state 96 keV above the $9/2^+$ state.

We have performed calculations for other odd-proton nuclei in the mass region, such as ^{95}Nb, and we have observed that in this reduced model space the negative-parity states are always lower in energy than observed experimentally. The misplacement in energy of these states cannot be corrected with an increase of the $\pi p_{1/2}$ SPE and therefore is a shortcoming of our calculation that could be also related with the two limitations discussed above. This can as well cause the large disagreement between experimental and calculated excitation energies for the high-spin positive-parity states above $33/2^+$.

4 Conclusions

A new in-beam γ-ray spectroscopy investigation of ^{97}Tc has been made with a heavy-ion fusion-evaporation reaction. This resulted in a significant expansion of the level scheme at high spins. Spherical shell model calculations in the $[\pi(p_{1/2}, g_{9/2}); \nu(d_{5/2}, g_{7/2}, d_{3/2}, s_{1/2})]$ space show an overall good agreement with the experimental data, with some limitations at the higher spins which indicate the need of enlarging the diagonalization space and, possibly, of breaking the considered inert core.

We are indebted to A. Brown for his advice and help with the shell model calculations.

References

1. B.W. Huber, K. Krämer, Z. Phys. A **267**, 111 (1974).
2. L.R. Medsker, T.H. Braid, J.L. Yntema, Phys. Lett. C **8**, 1425 (1973).
3. H.C. Cheung, J. Kitching, J.K.P. Lee, S.K. Mark, J. Phys. G **1**, 737 (1975).
4. S. Landsberger, R. Lecomte, P. Paradis, S. Monaro, Nucl. Phys. A **339**, 238 (1980).
5. G. Kajrys, S. Landsberger, R. Lecomte, P. Paradis, S. Monaro, Phys. Rev. C **26**, 1451 (1982).
6. H. Aslan, B. Crowe, T. Dague, D.G. Savage, S. Zeghib, F.A. Rickey, P.C. Simms, Phys. Rev. C **54**, 576 (1996).
7. G. Kajrys, M. Irshad, S. Landsberger, R. Lecomte, P. Paradis, S. Monaro, Phys. Rev. C **26**, 1462 (1982).
8. D. Hippe, H.W. Schuh, U. Kaup, K.O. Zell, P. von Brentano, Z. Phys. A **311**, 329 (1983).
9. S.S. Ghugre, B. Kharraja, U. Garg, R.V.F. Jansens, M.P. Carpenter, B. Crowell, T.L. Khoo, T. Lauritsen, D. Nisius, W. Reviol, W.F. Mueller, L.L. Riedinger, R. Kaczarowski, Phys. Rev. C **61**, 024302 (1999).
10. D. Bucurescu, Gh. Căta-Danil, I. Căta-Danil, M. Ivaşcu, N. Mărginean, C. Rusu, L. Stroe, C.A. Ur, A. Gizon, J. Gizon, B. Nyakó, J. Timár, L. Zolnai, A.J. Boston, D.T. Joss, E.S. Paul, A.T. Semple, M. Parry, Eur. Phys. J. A **10**, 255 (2001).
11. A. Bauchet, I. Deloncle, M.-G. Porquet, A. Astier, N. Buforn, M. Meyer, S. Perries, N. Redon, B.J.P. Gall, F. Hoellinger, N. Schulz, G. Duchêne, S. Courtin, Ts. Venkova, P.A. Butler, N. Amzal, R.D. Herzberg, A. Chewter, R. Cunningham, M. Houry, R. Lucas, W. Urban, A. Nowak, E. Piasecki, J. Duprat, C. Petrache, T. Kröll, Eur. Phys. J. A **10**, 145 (2001).
12. F. Iachello, O. Scholten, Phys. Rev. Lett. **43**, 679 (1979).
13. F. Iachello, A. Arima, *The Interacting Boson Model* (Cambridge University Press, Cambridge, 1987).
14. K.O. Zell, H. Harter, D. Hippe, H.W. Schuch, P. von Brentano, Z. Phys. A **316**, 351 (1984).
15. H.A. Smith jr., F.A. Rickey, Phys. Rev. C **14**, 1946 (1976).
16. R. Bengtsson, S. Frauendorf, Nucl. Phys. A **327**, 139 (1970).
17. R.P. Singh, R.K. Bhowmik, S.S. Ghugre, S.B. Patel, Eur. Phys. J. A **7**, 35 (2000).
18. B.A. Brown, A. Etchegoyen, W.D.M. Rae, N.S. Godwin, MSU-NSCL Report No. 524, 1985, unpublished.
19. H. Mach, E.K. Warburton, R.L. Gill, R.F. Casten, J.A. Becker, B.A. Brown, J.A. Wigner, Phys. Rev. C **41**, 226 (1990).
20. A. Hosaka, K.I. Kubo, H. Toki, Nucl. Phys. A **244**, 76 (1985).
21. D.H. Gloeckner, Nucl. Phys. A **253**, 301 (1975).